LANGMUIR Article
Cite This: *Langmuir* 2018, 34, 15084−15092
pubs.acs.org/Langmuir

Dynamic Interactions between Lipid-Tethered DNA and Phospholipid Membranes

Patrick M. Arnott,[†] Himanshu Joshi,[‡] Aleksei Aksimentiev,*[,‡] and Stefan Howorka*[,†]

[†]Department of Chemistry, Institute of Structural and Molecular Biology, University College London, London WC1H 0AJ, United Kingdom

[‡]Department of Physics, and Beckman Institute for Advanced Science and Technology, University of Illinois at Urbana−Champaign, Urbana, Illinois 61801, United States

Supporting Information

ABSTRACT: Lipid-anchored DNA can attach functional cargo to bilayer membranes in DNA nanotechnology, synthetic biology, and cell biology research. To optimize DNA anchoring, an understanding of DNA−membrane interactions in terms of binding strength, extent, and structural dynamics is required. Here we use experiments and molecular dynamics (MD) simulations to determine how the membrane binding of cholesterol-modified DNA depends on electrostatic and steric factors involving the lipid headgroup charge, duplexed or single-stranded DNA, and the buffer composition. The experiments distinguish between free and membrane vesicle-bound DNA and thereby reveal the surface density of anchored DNA and its binding affinity, something which had previously not been known. The K_d values range from 8.5 ± 4.9 to 466 ± 134 μM whereby negatively charged headgroups led to weak binding due to the electrostatic repulsion with respect to the negatively charged DNA. Atomistic MD simulations explain the findings and elucidate the dynamic nature of anchored DNA such as the mushroom-like conformation of single-stranded DNA hovering over the bilayer surface in contrast to a straight-up conformation of double-stranded DNA. The biophysical insight into the binding strength to membranes as well as the molecular accessibility of DNA for hybridization to molecular cargo is expected to facilitate the creation of biomimetic DNA versions of natural membrane nanopores and cytoskeletons for research and nanobiotechnology.

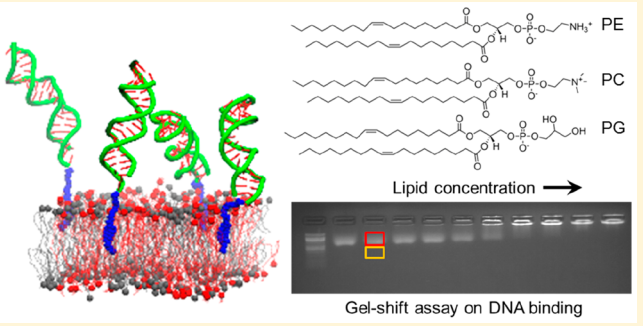

INTRODUCTION

A terminally attached lipid can anchor a DNA strand to bilayer membranes. This simple approach has impacted a range of research fields.[1] In biophysics, terminally anchored DNA permits the study of DNA hybridization in two-dimensional space compared to conventional hybridization in solution[2−5] and also allows the facile visualization of membrane regions.[6] In nanobiotechnology, lipid-linked DNA enables the hybridization-mediated attachment of functional cargo[7,8] at the fluid−lipid interface to mimic the function of proteins. For example, DNA-based artificial cytoskeletons can be used to shape membrane vesicles.[9−12] Similarly, DNA-based pores can be anchored to puncture the membrane[13−18] for applications such as biosensing[19−21] or controlled drug release.[17] Membrane-anchored DNA nanostructures can also probe membrane interaction forces[22] or alter the composition of a lipid bilayer membrane.[23] Finally, in synthetic biology, membrane-anchored DNA can link via duplex-formation vesicles to planar membrane[24] vesicles[2,25,26] or cells[27] often by assuming the function of membrane fusion proteins.[28−33]

Understanding the interaction of anchored DNA with bilayer membranes is important for basic science and attaining the desired performance in applications. For example, end-point-tethered DNA should be stably anchored to the membrane with high affinity. Furthermore, the DNA should be sterically accessible to enable hybridization with an incoming complementary DNA strand. This means that the DNA should neither cluster with each other nor adhere with its bases or backbone to the membrane. To understand DNA−membrane interactions, one study looked at changes in the hydrodynamic radii of DNA and the effect of multiple lipid anchors,[3] yet there are several unanswered questions. For example, what are the affinity and surface density of end-point-tethered DNA strands, and how do both depend on experimental parameters that influence electrostatic and sterics? Charge-relevant parameters are the ionic headgroup of phospholipids and the salt composition of the buffer. Another parameter that involves both electrostatics and sterics is the DNA length, for both the single- and double-stranded forms. Further questions relate to the dynamics and molecular

Special Issue: Nucleic Acids Nanoscience at Interfaces

Received: July 5, 2018
Revised: September 1, 2018
Published: October 10, 2018

DOI: 10.1021/acs.langmuir.8b02271
Langmuir 2018, 34, 15084−15092

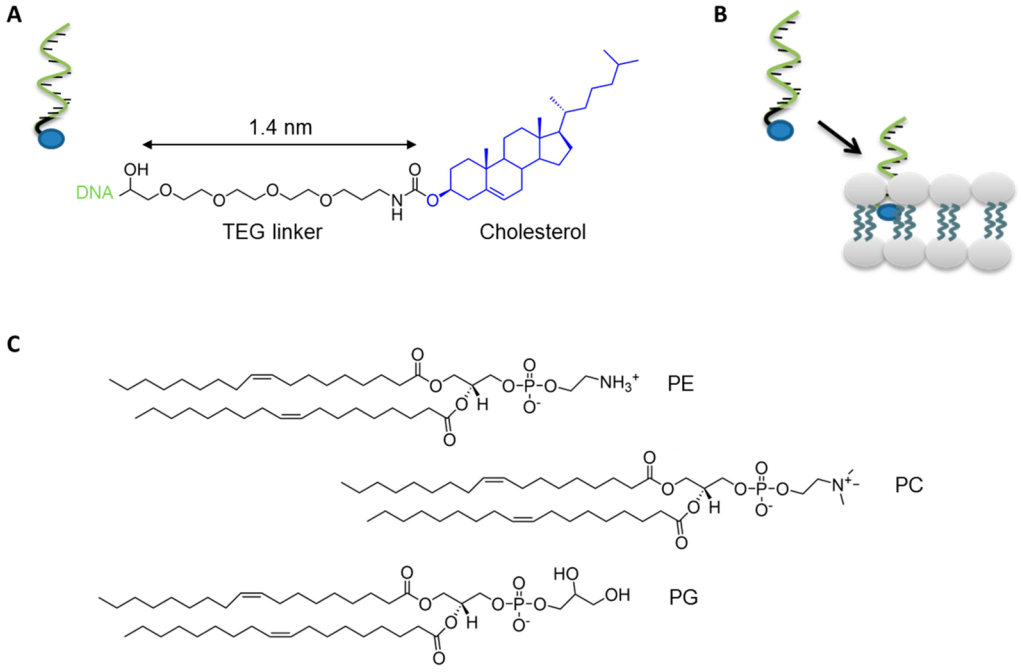

Figure 1. Molecular components used to probe the interaction between lipid-modified DNA and bilayer membranes. (A) DNA oligonucleotide carrying a 5′-terminal cholesterol via a TEG linker. (B) Schematic drawing of a cholesterol-modified DNA oligonucleotide inserted into a lipid bilayer. (C) Phospholipids 1,2-dioleoyl-*sn*-glycero-3-phosphoethanolamine (PE), 1,2-dioleoyl-*sn*-glycero-3-phosphocholine (PC), and 1,2-dioleoyl-*sn*-glycero-3-phospho-*rac*-(1′-glycerol) (PG).

visualization of terminally tethered DNA. For example, under which conditions does the remaining part of the DNA strand adhere to the lipid bilayer? Answering these questions would lead to a better understanding of how DNA and membranes interact and thereby form a rational basis to design targeted anchoring of DNA nanostructures or achieve defined contact between bilayers.

In this study, we use experiments and computation to examine how DNA strands with a single terminally tethered lipid anchor to and interact with synthetic lipid bilayer membranes (Figure 1A,B). The DNA oligonucleotides carry a cholesterol anchor tethered via a flexible tetra(ethylene glycol) (TEG) linker at the 5′ terminus of each strand (Figure 1A). To probe the length and sterics, both 20- and 40-nt-long oligonucleotides as well as double-stranded DNA (dsDNA) and single-stranded DNA (ssDNA) are examined. The synthetic membranes are small unilamellar vesicles (SUVs) of tunable lipid composition. The lipids were chosen on the basis of their wide use in research and to cover representative lipid headgroups ranging from negatively charged to zwitterionic with either a tertiary or a quaternary amine. The vesicles were composed of a 7:3 (ref 17) mixture of two phospholipids with the following zwitterionic headgroups: 1,2-dioleoyl-*sn*-glycero-3-phosphoethanolamine (DOPE, PE) and 1,2-dioleoyl-*sn*-glycero-3-phosphocholine (DOPC, PC) (Figure 1C). Alternatively, the membranes are a 4:1 mixture of PE and negatively charged 1,2-dioleoyl-*sn*-glycero-3-phospho-*rac*-(1′-glycerol) (DOPG, PG) (Figure 1C). In addition, the influence of two buffers is examined to probe the influences of salt composition and ionic strength. Phosphate-buffered saline (PBS) contains Na^+ (10 mM PO_4^{3-}, 154 mM NaCl) and has an ionic strength of 0.179 M at pH 7.4. As a comparison, a K^+-containing buffer of 0.3 M KCl and 15 mM Tris at pH 8.0 with an ionic strength of 0.315 M was also tested. The two buffering components (PO_4^{3-} vs amine- and alcohol-containing Tris) are different, yet their concentration is considerably lower than the alkali salt components which dominate the ionic character of the solutions. Furthermore, the pH of the buffers is similar and maintains the ionization of the lipid headgroups shown in Figure 1C.

In exploiting this wide chemical parameter space, the anchoring of cholesterol DNA to the SUVs is analyzed with gel electrophoresis to distinguish free and SUV-bound DNA and thereby infer the surface density of DNA on the membranes as well as the affinity of the interaction. Mirroring the system explored by experiment, we construct all-atom models of arrays of dsDNA or ssDNA molecules embedded in lipid bilayer membranes[34−36] via covalently attached cholesterol anchors. The systems are solvated with explicit electrolytes (ions and water), allowing for an accurate account of electrostatic interactions. The structures are animated using the molecular dynamics (MD) method that characterizes equilibrium and kinetic properties of lipid-tethered DNA systems.

Our quantitative studies establish that cholesterol−DNA can pack tightly on membranes with a maximum density of one strand per 0.02 to 0.04 nm^2, depending on the lipid composition. By comparison, the affinity varies by up to 50-fold depending on the lipid headgroup, DNA length, and buffer. Both data sets underscore the strong influence of electrostatics on the interaction of DNA and the lipid membrane. As an example, negatively charged lipids lead to weakened affinity while ssDNA is generally undergoing close contact with zwitterionic lipids. The simulations support the data and show the conformations of anchored DNA molecules on membranes. The detailed understanding can improve the designs of membrane-interacting DNA nanostructures such as by tuning the membrane affinity of DNA strands or by choosing conditions to enhance the molecular accessibility of DNA for hybridization to functional molecular cargo.

DOI: 10.1021/acs.langmuir.8b02271
Langmuir 2018, 34, 15084−15092

RESULTS

Analyzing the Interaction of Lipidated DNA and Membrane Vesicles with a Gel-Shift Assay. The binding of cholesterol-modified DNA strands to small unilamellar vesicles (SUVs) was assayed with agarose gel electrophoresis. DNA strands that were bound to the vesicles were separated from free DNA strands on the basis of the size-exclusion effect of the gel. The gel matrix is wide enough to permit the electrophoretic migration of unbound DNA oligonucleotides. However, 70 to 110 nm SUVs are too large for the matrix pores.

The principle of separating free from membrane-bound DNA helped to determine the extent of membrane binding. In the titration experiments, the number of vesicles, equivalent to the total surface area of membranes, was increased while the DNA concentration was held constant. The advantage of this method is that a constant DNA concentration facilitates the gel electrophoretic analysis of membrane-bound vs free DNA. The alternative method of keeping the membrane surface area constant would have led to greatly varying amounts of DNA that are difficult to analyze in gels with a limited linear range.

A typical read out of a titration experiment is shown in Figure 2A for 20-nt-long ssDNA and PE/PC vesicles in PBS buffer. At low SUV/lipid concentrations, most of the cholesterol–DNA was in the unbound form and migrated into the gel. Increasing SUV concentration led to more DNA binding and a higher proportion of DNA in the SUV band at the top of the gel (Figure 2A). No free DNA was present at the highest lipid concentration. The binding of DNA is mediated by cholesterol but not electrostatic interactions as DNA without a lipid anchor did not migrate at the SUV band (not shown).

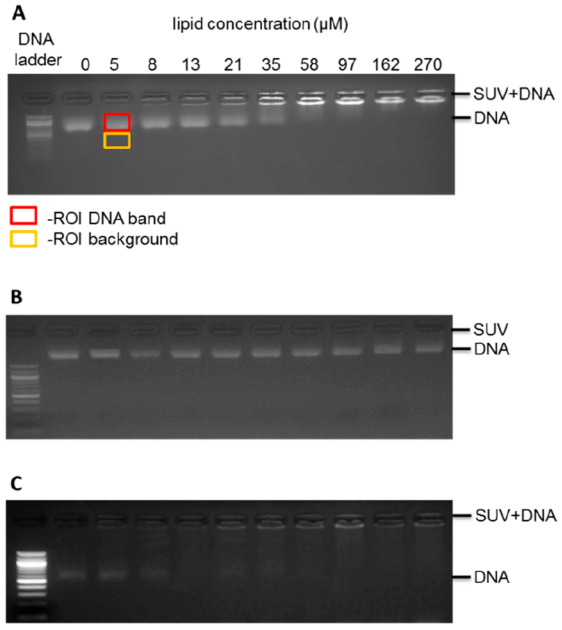

Figure 2. Gel-shift assay to determine the extent of membrane binding for cholesterol-modified DNA strands. The assay discriminates free DNA that migrates into the agarose gel and membrane vesicle-bound DNA at the top of the gel. Increasing the concentration of lipid membrane vesicles (0–250 μM lipid) changes the proportion of DNA from the free to the bound state. (A) Titration result for the binding of cholesterol-modified 20-nt ssDNA to PE/PC vesicles in PBS. The red box around the free DNA band was used to determine the band intensity which was corrected for the background of the gel (orange box). See the text for more details. (B) The titration read-out for 20-nt ssDNA against PE/PG in 0.3 M KCl reveals a weak extent of membrane binding. (C) A strong interaction is found for 20-nt dsDNA to PE/PG in PBS.

The gel-shift assay revealed strong changes in the extent of membrane binding of cholesterol–DNA. For example, changing the lipid headgroups from PE/PC (neutral) to PE/PG (negative) and replacing PBS with 0.3 M KCl resulted in an almost complete lack of binding; most DNA migrated into the gel even at the highest lipid concentration (Figure 2B). In contrast to very weak binding, the gel assay also established a strong interaction. As shown in Figure 2C, the same PE/PG vesicles except dsDNA and PBS led to stronger binding than in the previous cases. Under these conditions, the critical lipid concentration at which half of the DNA is fully incorporated into the SUV shifted to the left (compare Figure 2B,C). Hence, the gel-shift assay extracts information about the extent of cholesterol-mediated anchoring as a function of the membrane lipid headgroup, buffer, and DNA type.

Quantifying DNA Membrane Binding. The titration results were analyzed to obtain two quantitative measures of the DNA–bilayer interaction: the affinity and the maximum surface density of anchored DNA. Toward this end, gel images were subjected to ImageJ analysis. Band intensities for free DNA, I_{DNA}, were determined within a region of interest (ROI) around the band (Figure 2A, red box) and then by subtracting the background intensity of the gel, $I_{background}$ (Figure 2A, orange box). The data on $1 - (I_{DNA} - I_{background})$ were then plotted against the lipid concentration and fitted to a Langmuir isotherm (Figure 3). The affinity of the interaction, K_d, was inferred from the fits under the assumption that the varying area of the membrane surface does not influence the energetics of the membrane anchoring of DNA.

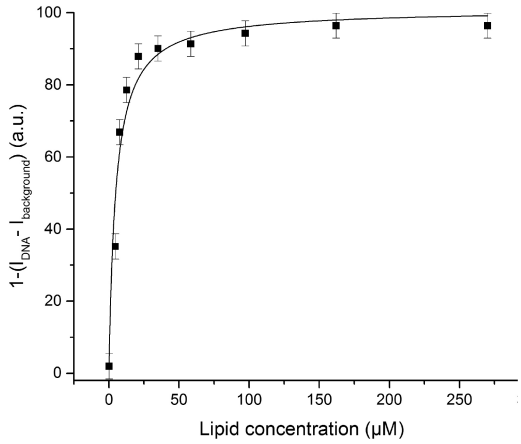

Figure 3. Quantitative analysis of the gel-shift data with a plot of the gel intensity-derived value of $1 - (I_{DNA} - I_{background})$, which is equivalent to the normalized amount of SUV-bound DNA vs the concentration of lipid used to generate SUVs. The analysis is for the binding of cholesterol-modified dsDNA of 20 nt to PE/PC vesicles in 0.3 M KCl. The averages and standard deviations represent data from three independent experiments.

The maximum surface density was derived in a two-step process by first dividing the amount of added DNA by the total membrane surface area using $\delta = DNA_{max}/(0.5A_l n_l T_s)$, where DNA_{max} is the maximum amount of DNA loaded onto the vesicles, n_l is the number of lipids per vesicle, T_s is the number

DOI: 10.1021/acs.langmuir.8b02271
Langmuir 2018, 34, 15084–15092

of SUVs, and A_l is the area occupied by a single lipid molecule depending on the lipid type.[37−40] The factor of 0.5 accounts for the double-leaflet structure of the bilayers. The values of δ were 0.03 molecules nm^{-2} for PE/PC and 0.04 molecules nm^{-2} for PE/PG vesicles.[3,41] In a second step, the maximum surface density was obtained by multiplying δ by the Langmuir fit-derived value of relative binding, i.e., $1 - (I_{DNA} - I_{background})$, under the assumption that 100% is equal to δ (Figure 3).

K_d and surface-density values were determined for DNA of both lengths (20 vs 40 nt), ssDNA and dsDNA, charge-neutral PE/PC membranes and predominately negatively polarized PE/PG membranes, and two buffer conditions (BPS and 0.3 M KCl). For each of these conditions, data were acquired in at least three independent experiments. The results of the quantitative analysis are shown in Figure 4 and Supporting Information, Table S1 and Figure S1..

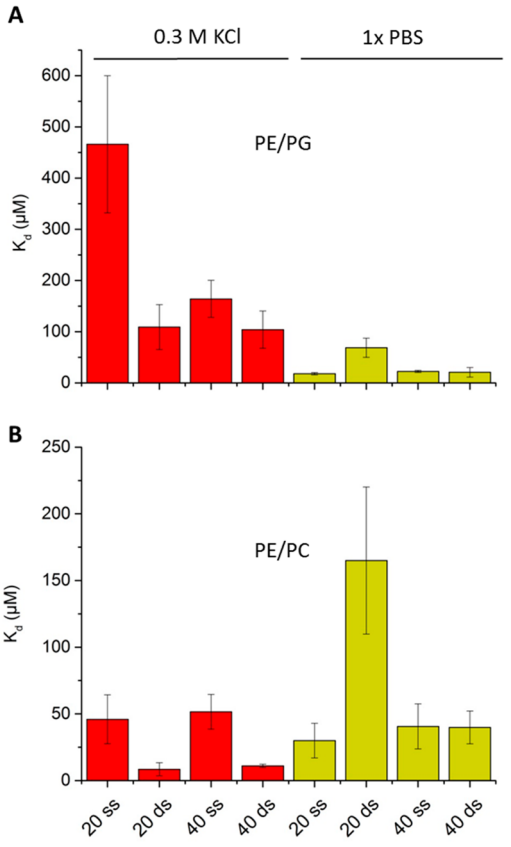

Figure 4. K_d values obtained from the gel-shift assay for DNA strands on PE/PG (A) and PE/PC SUVs (B) in a buffer of 0.3 M KCl (red columns) or PBS (yellow columns).

The maximum surface density ranged from 0.029 ± 0.001 to 0.047 ± 0.005 molecules nm^{-2} for all conditions tested, with the majority around 0.03 molecules nm^{-2} (Figure S1 and Table S1). There is no clear systematic trend in how the surface density depended on a single set of parameters composed of a lipid headgroup, a buffer, and a DNA length.

Lower Affinity of Lipid-Anchored DNA for Membranes with Negatively Charged Lipids and the Influence of Buffer Composition. In contrast to the modestly variable surface densities, the K_d for the membrane binding of cholesterol−DNA changed by up to 50-fold (Figure 4A,B, Table S1). A strong influencing factor was the membranes' lipid headgroup. Each of the four DNA types was bound with a higher affinity (low K_d) to PE/PC than to PE/PG membranes (Figure 4A,B, respectively; red bars; note the different y axis) in 0.3 M KCl buffer. The lower affinity is due to electrostatic repulsion between the negatively charged lipid headgroups and the phosphate groups in the backbone, as confirmed by simulations (see below).

The buffer composition also influenced the affinity. The binding on negative PE/PG membranes was weaker in 0.3 M KCl than in PBS (Figure 4A,B, respectively; yellow bars) when the four DNA types are compared side by side. The lower affinity in 0.3 M KCl is surprising because the buffer's higher ionic strength could have been expected to electrostatically screen DNA's phosphates more effectively than PBS and thereby reduce the electrostatic repulsion and increase the affinity. As the experimental affinity is higher in PBS, it is more probable that the different ionic composition (Na^+ vs K^+) of the buffers is the molecular reason.

Ion-exchange experiments[42] and all-atom MD simulations[43] have shown that Na^+ and K^+ ions have, overall, similar affinities for dsDNA molecules but bind to different parts of the molecule: minor (Na^+) and major (K^+) grooves in the DNA.[43,44] At the same time, previous MD simulations have found Na^+ ions to interact more strongly with the zwitterionic headgroups of PE and PC lipid bilayers[45,46] and reduce the average area per lipid headgroup. Our own MD simulations (Figure S2) also found Na^+ ions to screen the charge of PG headgroups as efficient as K^+ ions at double concentration and reduce the headgroup area. Thus, the net outcome of such an interaction can be quite complex because it depends on the ion-type-dependent screening of the DNA charge-, ion-, and lipid-headgroup-type-dependent screening of the membrane charge, ion type-dependent compression of the membrane, and conformation of the DNA molecule.

Indeed, we find the affinity of DNA to the lipid membrane also depends on whether DNA is single- or double-stranded. For example, dsDNA has a higher affinity than ssDNA of the same length on both PE/PC and PE/PG membranes despite carrying double the negative charge (Figure 4A,B, respectively; red bars). We attribute this behavior to the differences in the DNA conformation: a mushroom-like conformation of ssDNA brings its negative charges closer, on average, to the membrane than the straight-up conformation of dsDNA. (See the simulation results in Figure 5A,B.) However, this is only the case for 0.3 M KCl, whereas in PBS there is no uniform trend (Figure 4A,B, yellow bars). Such a buffer dependence could be explained by better screening of the electrical charges in the case of the PBS buffer, which would lessen the electrostatic penalty for both molecules. Overall, the data suggest that the dependence of the affinity on the lipid headgroup and buffer type can be rationalized by considering electrostatic interactions between DNA and membrane headgroups and by the additional influence of buffer composition on charge screening. However, in several cases, the interplay between the factors is more complex and requires considerations of the conformation and length of the DNA strand.

Visualization of DNA Tethering to Lipid Bilayers through MD Simulations. To elucidate the microscopic configurations adopted by DNA molecules tethered to different lipid bilayers, we built six all-atom models of the experimental systems (Figure 5). Each system contained four copies of either dsDNA or ssDNA molecules conjugated to a cholesterol linker, a patch of a pure POPE (PE) membrane, or

DOI: 10.1021/acs.langmuir.8b02271
Langmuir 2018, 34, 15084−15092

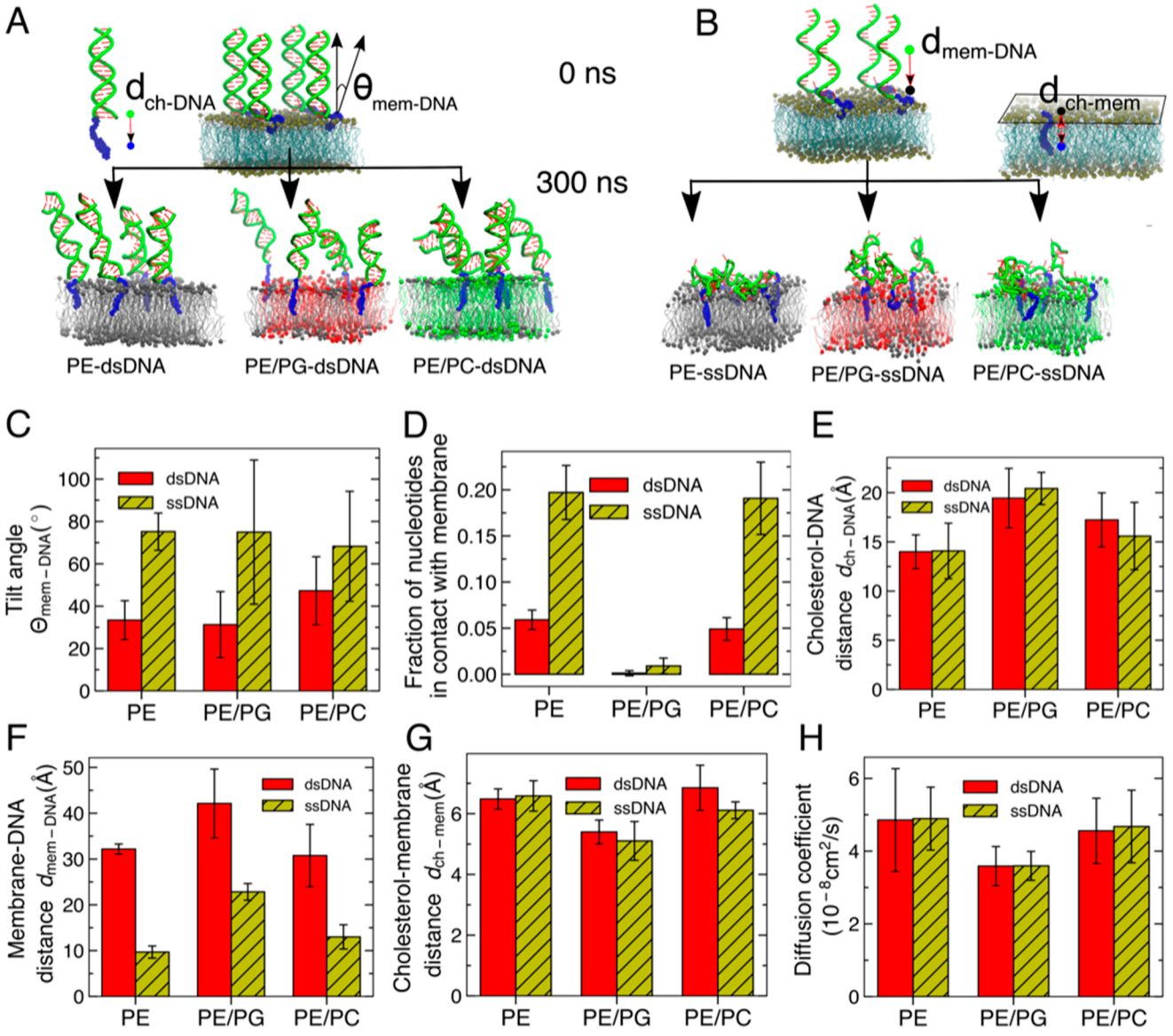

Figure 5. Molecular dynamics simulations of DNA tethered to lipid bilayer membranes. (A, B) Initial (top) and final (bottom) configurations of the simulation systems. Each system contains four DNA molecules with 20 base pairs (panel A) or nucleotides (panel B). Each molecule is tethered to the lipid bilayers through a cholesterol linker containing an additional nucleotide. The systems are immersed in 0.3 M KCl solution (not shown). (C) Average tilt of the DNA molecules with respect to the bilayer normal, $\theta_{\text{mem-DNA}}$. (D) Fraction of DNA nucleotides in contact with the lipid bilayer within the last 30 ns of the respective equilibration trajectory. A contact was defined as having a C3′ atom of a DNA backbone located within 5 Å of any nonhydrogen atoms in the membrane. (E) Average distance between cholesterol and the nearest dsDNA base pair or the second-nearest ssDNA nucleotide, $d_{\text{ch-DNA}}$. (F) Average distance between the DNA molecules and the nearest (upper) leaflet of the membrane, $d_{\text{mem-DNA}}$. (G) Average distance between cholesterol and the phosphate group of the membrane's upper leaflet, $d_{\text{ch-mem}}$. All distances reported in panels E–G were computed using center-of-mass coordinates of the respective groups projected along the bilayer normal and averaged over the last 200 ns of the equilibration trajectories. (H) Diffusion coefficient of cholesterol anchors in different membrane systems. SI Figures S4–S9 illustrate how the above quantities change with simulation time. The error bars show the standard deviation in the averaged values among the four DNA molecules in each simulation system.

a patch of a 50/50 POPE/POPG (PE/PG) or POPE/POPC (PE/PC) lipid mixture and 300 mM KCl solution (top panels in Figure 5A,B). The six systems were equilibrated for 300 ns each, and the final configurations of the DNA molecules are shown in the bottom panels of Figure 5A,B. See Methods for a detailed description of the simulation protocols.

During the MD simulations, the configuration of DNA molecules deviated significantly from their initial idealized conformations (Figure 5A,B, Figure S3, and Movies 1–6). Significant differences in the conformations of dsDNA and ssDNA can be seen regardless of the lipid bilayer type: while dsDNA molecules maintained largely upright conformations (Figure 5C and Figure S4), ssDNA molecules collapsed, forming a polymer brush. The propensity of DNA molecules to form contacts with lipid bilayer membranes clearly depended not only on the type of DNA molecules (ssDNA versus dsDNA) but also on the lipid bilayer composition (Figure 5D and Figure S5). Thus, more than 20% of all nucleotides of ssDNA formed stable contacts with the headgroups of PE or PE/PC bilayers, whereas the presence of PG headgroups prevented such contacts from forming. The differential affinity of DNA molecules to the lipid bilayer containing 50% PG

DOI: 10.1021/acs.langmuir.8b02271
Langmuir 2018, 34, 15084–15092

headgroups is explained by the negative charge of the PG groups, which repels negatively charged DNA.

The composition of a lipid bilayer is found to have a measurable effect on the manner in which the DNA−cholesterol conjugates are anchored to the membrane. The repulsive electrostatic interaction between DNA and PG headgroups produced stretching of the linker, increasing the distance between the cholesterol moiety and the proximal fragments of DNA in comparison to the configurations observed for pure PE or PE/PC membrane systems (Figure 5E and Figure S6). The effect becomes even more significant when looking at the average distance between the lipid headgroups and the proximal fragments of DNA (Figure 5F and Figure S7). Conversely, cholesterol anchors are found to be located closer to the lipid headgroups in the case of the PE/PG bilayer (Figure 5G and Figure S8). All of the above suggest that the composition of lipid membranes can have a considerable effect on the stability of cholesterol-anchored DNA molecules and that DNA tethering to PE/PG mixture is less stable than to pure PE or mixed PE/PC membranes. These conclusions apply to both dsDNA and ssDNA.

Finally, we note that, while being tethered to lipid bilayers, the DNA molecules are free to diffuse along the membrane surface. Figure 5H plots the diffusion constants of the cholesterol anchors linked to ssDNA and dsDNA molecules in the lipid membranes of the three compositions. The diffusion of the anchors is found to be similar for ssDNA- and dsDNA-conjugated molecules, suggesting that that resistance of the lipid bilayer determines the rate of diffusion of the cholesterol−DNA complexes. At the same time, we find the diffusion of cholesterol anchors in the PE/PG membrane to be slower than that in pure PE or PE/PC mixture membranes. We attribute this observation to a shallower placement of the anchors in the PE/PG membrane (Figure 5G). Indeed, rich in hydrogen bonds and salt-bridge interactions, the lipid headgroup environment can be expected to provide more resistance to cholesterol diffusion than can the hydrophobic environment of lipid tails.

CONCLUSIONS

Given the versatile use of membrane-tethered DNA in several research areas, this study has examined how cholesterol-modified DNA strands anchor and interact with lipid bilayers. Biophysical insight is relevant and can guide the future design of membrane-interacting DNA nanostructures such as by tuning the membrane affinity of DNA strands or by choosing conditions to enhance the molecular accessibility of DNA for hybridization to functional molecular cargo.

First, the K_d values of DNA lipid-anchored to membranes are reported. Previously, this important biophysical data was not known. Second, the ionic interaction is a main factor influencing membrane tethering. Electrostatic repulsion between negatively charged DNA and similarly charged lipid headgroups strongly reduces the affinity of the interaction. Electrostatic screening of negative charges by counterions can compensate for this effect. Microscopic visualization with molecular dynamics concurs and adds further insight into the role of electrostatics. Repulsion leads to minimal contact between DNA and the membrane, increased stretching of DNA and the linker relative to the membrane-inserted cholesterol, and slower lateral diffusion of DNA in the membrane.

In addition to electrostatics, this study underscores the role of sterics. In molecular visualization, single- vs double-stranded DNA exhibits different dynamic structures on membranes. While dsDNA molecules maintain largely upright conformations, ssDNA molecules collapse to form a polymer brush. The collapse is accompanied by increased contact with the membrane, provided there are positive charges in the lipid headgroups. The conformational differences between single- and double-stranded DNA are expected to influence the respective molecular accessibility on membrane interfaces.

By synergistically combining experiment and computational simulations, the new insight can be used by researchers in the field of DNA nanotechnology or biophysics to improve the design of DNA strands or the choice of lipids to facilitate hybridization at membranes. For example, if single-stranded DNA is used, then negatively charged as opposed to zwitterionic lipids are suggested to lead to more steric accessibility of the bases for hybridization, although at the cost of a lower affinity of membrane anchoring. Furthermore, because double-stranded DNA has the weakest backbone interaction with the membranes, another practically relevant suggestion is to attain DNA hybrdiziation with a new strand via toe-hold-mediated strand displacement as opposed to simple single-strand association. In conclusion, our report delivers fundamental scientific insight into DNA at bilayer interfaces and provides a new scope for the development of DNA nanotechnology and synthetic biology.

METHODS

Materials. Unmodified and cholesterol-labeled DNA oligonucleotides were purchased from Integrated DNA Technologies on a 100 nmol scale with HPLC or PAGE purification. 1,2-Dioleoyl-*sn*-glycero-3-phosphoethanolamine (PE), 1,2-dioleoyl-*sn*-glycero-3-phosphocholine (PC), and 1,2-dioleoyl-*sn*-glycero-3-phospho-(1′-*rac*-glycerol) (PG) were procured from Avanti Polar Lipids. All other reagents and solvents were purchased from Sigma-Aldrich.

DNA Duplex Formation. DNA oligonucleotides were dissolved in deionized water at a concentration of 100 μM prior to dilution in buffers PBS (10 mM PO_4^{3-}, 154 mM NaCl, pH = 7.4) or KCl (0.3 M KCl, 15 mM Tris, pH 8.0). DNA duplexes were obtained by preparing an equimolar mixture of DNA strands at a final concentration of 10 μM and incubating the mixture for 2 min at 95 °C, followed by cooling to 20 °C at a rate of 5 °C per min using a PCR thermocycler. The sequences of the DNA oligonucleotides are 20 nt 5′-TAG TCG ATT TTA TCC ATG CA-TEG-cholesterol-3′, 20 nt compliment 5′-TGC ATG GAT AAA ATC GAC TA-3′, 40 nt 5′-CAT TTT TCC ACG TTC GCT AAT AGT CGA TTT TAT CCA TGC A-TEG-cholesterol-3′, and 40 nt compliment 5′-TGC ATG GAT AAA ATC GAC TAT TAG CGA ACG TGG AAA AAT G-3′.

Preparation of SUVs. A solution of lipids PE (0.3 mmol, 50 μL) and PC (0.7 mmol, 550 μL) or PG (0.2 mmol, 100 μL) and PE (0.8 mmol, 59.5 μL) in chloroform was added to a 5 mL round-bottomed flask. The solvent was removed using a rotary evaporator to yield a thin film, which was subsequently dried under ultrahigh vacuum for 3 h. The lipid was resuspended in a buffer of 0.3 M KCl and 15 mM Tris at pH 8.0 or PBS (1 mL), and the solution was sonicated for 30 min at room temperature. SUVs were left to equilibrate for 5 h and were used within 24 h. The suspension was gently resuspended 2 s before use. SUVs were subjected to dynamic light scattering (DLS) to confirm the vesicles' diameter using a Zetasizer Nano S from Malvern. The diameters and PDIs were 69 ± 8 nm and 0.23 for PE/PG and 106 ± 3 nm and 0.76 for PE/PC vesicles, respectively.

DNA−SUV Binding Assay and Agarose Gel Electrophoresis. The binding assay was conducted by mixing DNA solutions (10 μM, 10 μL; 20 ss, 20 ds, 40 ss, or 40 ds) with a suspension of PC/PE or PG/PE vesicles (1 mM lipid, 0−21.6 μL, end concentration 0−250

DOI: 10.1021/acs.langmuir.8b02271
Langmuir 2018, 34, 15084−15092

μM). The DNA SUV mixture was incubated for 20 min at room temperature. The mixture was analyzed using 2% agarose gel in TAE buffer at pH 8.0. To load samples on the gel, the DNA SUV mixture (40 μL) was combined with a solution (10 μL) of 60% glycerol. The gel was run at 60 V for 60 min at 20 °C. The bands were visualized by ultraviolet illumination after staining with ethidium bromide solution. A 100-base-pair marker (New England Biolabs) was used as the reference standard.

MD Methods. All-atom models of dsDNA and ssDNA molecules were created using the NAB module of AmberTools.[47] An additional nucleotide was added to DNA to covalently conjugate the cholesterol molecule via the TEG linker as described previously.[48] The initial configurations of the lipid bilayer membrane were generated from the CHARMM-GUI membrane builder.[49] Three types of membrane systems were built, each containing a 10 nm × 10 nm patch of either a pure POPE (PE) membrane or a 50/50 mixture of POPE/POPG (PE/PG) or POPE/POPC (PE/PC) lipids. Next, the four cholesterol-modified DNA molecules were merged with the lipid membranes by placing cholesterol anchors below the plane of lipid headgroups of the nearest leaflet and arranging the DNA molecules, within the membrane plane, on a square of 5 nm on a side. All lipid molecules located within 3 Å of the DNA atoms were removed. The systems were then solvated with TIP3P water[50] using the Solvate plugin of VMD;[51] potassium and chloride ions were added to produce an electrically neutral solution of 0.3 M salt concentration using an Autoionize plugin of VMD.[51] The final structures contained approximately 150 000 atoms.

The assembled systems were subjected to energy minimization using the conjugate gradient method that removed steric clashes between the solute and solvent atoms. During the minimization, all non-hydrogen atoms of DNA and the membrane were harmonically restrained to their initial coordinates (with a spring constants of 1 kcal/mol Å^{-2}). Subsequently, each system was equilibrated at a constant number of atoms (N), constant pressure (P = 1 bar), and constant temperature (T = 300 K), i.e., an NPT ensemble without any restraints. The Nose−Hoover Langevin piston[52,53] and Langevin thermostat were used to maintain the constant pressure and temperature in the system.[54] CHARMM36 force field parameters described the bonded and nonbonded interactions among DNA, lipid bilayer membranes, water, and ions[55] along with NBFIX corrections for nonbonded interactions.[56−58] Parameters for the cholesterol anchor were obtained using the CHARMM general force fields.[59] All-atom equilibrium MD simulations were performed using the NAMD2 program with periodic boundary conditions and the particle mesh Ewald (PME) method to calculate the long-range electrostatic interactions.[60] A 8−10−12 Å cutoff scheme was used to calculate van der Waals and short-range electrostatic forces. All simulations were performed using 2−2−6 multiple time steps for integrating the equation of motion. The SETTLE algorithm[61] was applied to keep water molecules rigid whereas the RATTLE algorithm[62] constrained all other covalent bonds involving hydrogen atoms. A 300 ns equilibrium MD simulation was performed for each system, which we found to be sufficient for the four DNA molecules to adopt statistically similar equilibrium conformations. The coordinates of the system were saved in the interval of the 9.6 ps simulation. The analysis and postprocessing of the simulation trajectories were performed using VMD[51] and CPPTRAJ.[63]

■ ASSOCIATED CONTENT

Supporting Information

The Supporting Information is available free of charge on the ACS Publications website at DOI: 10.1021/acs.langmuir.8b02271.

A table with the values of maximum surface density and K_d obtained from the gel shift assay; a histogram summarizing the values of maximum surface density and K_d obtained from the gel shift assay; molecular graphics images illustrating the conformations of dsDNA and ssDNA molecules observed in MD simulations; graphs detailing the effect of the ion type on screening the charge of a PE/PG membrane; additional molecular graphic images illustrating representative conformations of tethered DNA; graphs illustrating the dependence of the following quantities on the simulation time: the average tilt of the DNA molecules, the fraction of DNA in contact with the membrane, the distance between cholesterol and membrane, the distance between the membrane and DNA, the distance between cholesterol and the membrane, and the mean-squared displacement of the cholesterol anchor (PDF)

All-atom molecular dynamics simulation of dsDNA molecules cholesterol-anchored to a POPE lipid bilayer membrane (MPG)

All-atom molecular dynamics simulation of dsDNA molecules cholesterol-anchored to a lipid membrane composed of a 50/50 mixture of POPE and POPG lipids (MPG)

All-atom molecular dynamics simulation of dsDNA molecules cholesterol-anchored to a lipid membrane composed of a 50/50 mixture of POPE and POPC lipids (MPG)

All-atom molecular dynamics simulation of ssDNA molecules cholesterol-anchored to a POPE lipid bilayer membrane (MPG)

All-atom molecular dynamics simulation of ssDNA molecules cholesterol-anchored to a lipid membrane composed of a 50/50 mixture of POPE and POPG lipids (MPG)

All-atom molecular dynamics simulation of ssDNA molecules cholesterol-anchored to a lipid membrane composed of a 50/50 mixture of POPE and POPC lipids (MPG)

■ AUTHOR INFORMATION

Corresponding Authors

*E-mail: aksiment@illinois.edu.

*E-mail: s.howorka@ucl.ac.uk.

ORCID

Aleksei Aksimentiev: 0000-0002-6042-8442

Stefan Howorka: 0000-0002-6527-2846

Funding

S.H. and P.M.A. acknowledge support by the National Physical Laboratory. S.H. is supported by the EPSRC (EP/N009282/1), the BBSRC (BB/M025373/1 and BB/N017331/1), and the Leverhulme Trust (RPG-2017-015). A.A. and H.J. acknowledge support from the National Science Foundation under grants DMR-1827346 and DMR-1507985, the National Institutes of Health under grant P41-GM104601, the supercomputer time provided through XSEDE allocation grant MCA05S028, and the Blue Waters petascale supercomputer system (UIUC). H.J. acknowledges Govt. of India for the DST-Overseas Visiting Fellowship in Nano Science and Technology.

Notes

The authors declare no competing financial interest.

■ ACKNOWLEDGMENTS

We thank Conor Lanphere for contributing to the literature research and calculating the surface density of DNA and

DOI: 10.1021/acs.langmuir.8b02271
Langmuir 2018, 34, 15084−15092

Christoph Salzmann for discussing the biophysical analysis of membrane binding.

■ ABBREVIATIONS

DNA, deoxyribose nucleic acid; HPLC, high-pressure liquid chromatography; PAGE, polyacrylamide gel electrophoresis; PC, 1,2-dioleoyl-*sn*-glycero-3-phosphocholine; PE, 1,2-dioleoyl-*sn*- glycero-3-phosphoethanolamine; PG, 1,2-dioleoyl-*sn*-glycero-3-phospho-*rac*-(1′-glycerol); SUV, small unilamellar vesicle

■ REFERENCES

(1) Lopez, A.; Liu, J. DNA Oligonucleotide-Functionalized Liposomes: Bioconjugate Chemistry, Biointerfaces, and Applications. *Langmuir* **2018**, DOI: 10.1021/acs.langmuir.8b01368.
(2) Yoshina-Ishii, C.; Boxer, S. G. Arrays of Mobile Tethered Vesicles on Supported Lipid Bilayers. *J. Am. Chem. Soc.* **2003**, *125*, 3696−3697.
(3) Banchelli, M.; Gambinossi, F.; Durand, A.; Caminati, G.; Brown, T.; Berti, D.; Baglioni, P. Modulation of Density and Orientation of Amphiphilic DNA on Phospholipid Membranes. Ii. Vesicles. *J. Phys. Chem. B* **2010**, *114*, 7348−7358.
(4) Gambinossi, F.; Banchelli, M.; Durand, A.; Berti, D.; Brown, T.; Caminati, G.; Baglioni, P. Modulation of Density and Orientation of Amphiphilic DNA Anchored to Phospholipid Membranes. I. Supported Lipid Bilayers. *J. Phys. Chem. B* **2010**, *114*, 7338−7347.
(5) Schade, M.; Berti, D.; Huster, D.; Herrmann, A.; Arbuzova, A. Lipophilic Nucleic Acids–a Flexible Construction Kit for Organization and Functionalization of Surfaces. *Adv. Colloid Interface Sci.* **2014**, *208*, 235−251.
(6) Loew, M.; Springer, R.; Scolari, S.; Altenbrunn, F.; Seitz, O.; Liebscher, J.; Huster, D.; Herrmann, A.; Arbuzova, A. Lipid Domain Specific Recruitment of Lipophilic Nucleic Acids: A Key for Switchable Functionalization of Membranes. *J. Am. Chem. Soc.* **2010**, *132*, 16066−16072.
(7) Jungmann, R.; Steinhauer, C.; Scheible, M.; Kuzyk, A.; Tinnefeld, P.; Simmel, F. C. Single-Molecule Kinetics and Super-Resolution Microscopy by Fluorescence Imaging of Transient Binding on DNA Origami. *Nano Lett.* **2010**, *10*, 4756−4761.
(8) Iinuma, R.; Ke, Y.; Jungmann, R.; Schlichthaerle, T.; Woehrstein, J. B.; Yin, P. Polyhedra Self-Assembled from DNA Tripods and Characterized with 3d DNA-Paint. *Science* **2014**, *344*, 65−69.
(9) Langecker, M.; Arnaut, V.; List, J.; Simmel, F. C. DNA Nanostructures Interacting with Lipid Bilayer Membranes. *Acc. Chem. Res.* **2014**, *47*, 1807−1815.
(10) Zhang, Z.; Yang, Y.; Pincet, F.; M, C. L.; Lin, C. Placing and Shaping Liposomes with Reconfigurable DNA Nanocages. *Nat. Chem.* **2017**, *9*, 653−659.
(11) Birkholz, O.; Burns, J. R.; Richter, C. P.; Psathaki, O. E.; Howorka, S.; Piehler, J. Multi-Functional DNA Nanostructures That Puncture and Remodel Lipid Membranes into Hybrid Materials. *Nat. Commun.* **2018**, *9*, 1521.
(12) Franquelim, H. G.; Khmelinskaia, A.; Sobczak, J. P.; Dietz, H.; Schwille, P. Membrane Sculpting by Curved DNA Origami Scaffolds. *Nat. Commun.* **2018**, *9*, 811.
(13) Langecker, M.; Arnaut, V.; Martin, T. G.; List, J.; Renner, S.; Mayer, M.; Dietz, H.; Simmel, F. C. Synthetic Lipid Membrane Channels Formed by Designed DNA Nanostructures. *Science* **2012**, *338*, 932−936.
(14) Howorka, S. Nanotechnology. Changing of the Guard. *Science* **2016**, *352*, 890−891.
(15) Burns, J.; Stulz, E.; Howorka, S. Self-Assembled DNA Nanopores That Span Lipid Bilayers. *Nano Lett.* **2013**, *13*, 2351−2356.
(16) Gopfrich, K.; Zettl, T.; Meijering, A. E.; Hernandez-Ainsa, S.; Kocabey, S.; Liedl, T.; Keyser, U. F. DNA-Tile Structures Induce Ionic Currents through Lipid Membranes. *Nano Lett.* **2015**, *15*, 3134−3138.
(17) Burns, J. R.; Seifert, A.; Fertig, N.; Howorka, S. A Biomimetic DNA-Based Channel for the Ligand-Controlled Transport of Charged Molecular Cargo across a Biological Membrane. *Nat. Nanotechnol.* **2016**, *11*, 152−156.
(18) Maingi, V.; Burns, J. R.; Uusitalo, J. J.; Howorka, S.; Marrink, S. J.; Sansom, M. S. Stability and Dynamics of Membrane-Spanning DNA Nanopores. *Nat. Commun.* **2017**, *8*, 14784.
(19) Howorka, S.; Siwy, Z. Nanopore Analytics: Sensing of Single Molecules. *Chem. Soc. Rev.* **2009**, *38*, 2360−2384.
(20) Liu, L.; Wu, H. C. DNA-Based Nanopore Sensing. *Angew. Chem., Int. Ed.* **2016**, *55*, 15216−15222.
(21) Stoloff, D. H.; Wanunu, M. Recent Trends in Nanopores for Biotechnology. *Curr. Opin. Biotechnol.* **2013**, *24*, 699−704.
(22) Dutta, P. K.; Zhang, Y.; Blanchard, A. T.; Ge, C.; Rushdi, M.; Weiss, K.; Zhu, C.; Ke, Y.; Salaita, K. Programmable Multivalent DNA-Origami Tension Probes for Reporting Cellular Traction Forces. *Nano Lett.* **2018**, *18*, 4803.
(23) Ohmann, A.; Li, C. Y.; Maffeo, C.; Al Nahas, K.; Baumann, K. N.; Gopfrich, K.; Yoo, J.; Keyser, U. F.; Aksimentiev, A. A Synthetic Enzyme Built from DNA Flips 10(7) Lipids Per Second in Biological Membranes. *Nat. Commun.* **2018**, *9*, 2426.
(24) Chung, M.; Boxer, S. G. Stability of DNA-Tethered Lipid Membranes with Mobile Tethers. *Langmuir* **2011**, *27*, 5492−5497.
(25) Ries, O.; Loffler, P. M.; Vogel, S. Convenient Synthesis and Application of Versatile Nucleic Acid Lipid Membrane Anchors in the Assembly and Fusion of Liposomes. *Org. Biomol. Chem.* **2015**, *13*, 9673−9680.
(26) Beales, P. A.; Vanderlick, T. K. Specific Binding of Different Vesicle Populations by the Hybridization of Membrane-Anchored DNA. *J. Phys. Chem. A* **2007**, *111*, 12372−12380.
(27) Peng, R.; Wang, H.; Lyu, Y.; Xu, L.; Liu, H.; Kuai, H.; Liu, Q.; Tan, W. Facile Assembly/Disassembly of DNA Nanostructures Anchored on Cell-Mimicking Giant Vesicles. *J. Am. Chem. Soc.* **2017**, *139*, 12410−12413.
(28) Stengel, G.; Zahn, R.; Hook, F. DNA-Induced Programmable Fusion of Phospholipid Vesicles. *J. Am. Chem. Soc.* **2007**, *129*, 9584−9585.
(29) Flavier, K. M.; Boxer, S. G. Vesicle Fusion Mediated by Solanesol-Anchored DNA. *Biophys. J.* **2017**, *113*, 1260−1268.
(30) van Lengerich, B.; Rawle, R. J.; Bendix, P. M.; Boxer, S. G. Individual Vesicle Fusion Events Mediated by Lipid-Anchored DNA. *Biophys. J.* **2013**, *105*, 409−419.
(31) Beales, P. A.; Vanderlick, T. K. Application of Nucleic Acid-Lipid Conjugates for the Programmable Organisation of Liposomal Modules. *Adv. Colloid Interface Sci.* **2014**, *207*, 290−305.
(32) Beales, P. A. Biophysics: A Toehold in Cell Surface Dynamics. *Nat. Nanotechnol.* **2017**, *12*, 404−406.
(33) Loffler, P. M. G.; Ries, O.; Rabe, A.; Okholm, A. H.; Thomsen, R. P.; Kjems, J.; Vogel, S. A DNA-Programmed Liposome Fusion Cascade. *Angew. Chem., Int. Ed.* **2017**, *56*, 13228−13231.
(34) Ash, W. L.; Zlomislic, M. R.; Oloo, E. O.; Tieleman, D. P. Computer Simulations of Membrane Proteins. *Biochim. Biophys. Acta, Biomembr.* **2004**, *1666*, 158−189.
(35) Piggot, T. J.; Pineiro, A.; Khalid, S. Molecular Dynamics Simulations of Phosphatidylcholine Membranes: A Comparative Force Field Study. *J. Chem. Theory Comput.* **2012**, *8*, 4593−4609.
(36) Khalili-Araghi, F.; Gumbart, J.; Wen, P. C.; Sotomayor, M.; Tajkhorshid, E.; Schulten, K. Molecular Dynamics Simulations of Membrane Channels and Transporters. *Curr. Opin. Struct. Biol.* **2009**, *19*, 128−137.
(37) Petrache, H. I.; Dodd, S. W.; Brown, M. F. Area Per Lipid and Acyl Length Distributions in Fluid Phosphatidylcholines Determined by (2)H Nmr Spectroscopy. *Biophys. J.* **2000**, *79*, 3172−3192.
(38) Fogarty, J. C.; Arjunwadkar, M.; Pandit, S. A.; Pan, J. Atomically Detailed Lipid Bilayer Models for the Interpretation of Small Angle Neutron and X-Ray Scattering Data. *Biochim. Biophys. Acta, Biomembr.* **2015**, *1848*, 662−672.

DOI: 10.1021/acs.langmuir.8b02271
Langmuir 2018, 34, 15084−15092

(39) Chiu, S. W.; Pandit, S. A.; Scott, H. L.; Jakobsson, E. An Improved United Atom Force Field for Simulation of Mixed Lipid Bilayers. *J. Phys. Chem. B* **2009**, *113*, 2748−2763.
(40) Harper, P. E.; Mannock, D. A.; Lewis, R. N.; McElhaney, R. N.; Gruner, S. M. X-Ray Diffraction Structures of Some Phosphatidylethanolamine Lamellar and Inverted Hexagonal Phases. *Biophys. J.* **2001**, *81*, 2693−2706.
(41) Banchelli, M.; Gambinossi, F.; Durand, A.; Caminati, G.; Brown, T.; Berti, D.; Baglioni, P. Modulation of Density and Orientation of Amphiphilic DNA on Phospholipid Membranes. Ii. Vesicles. *J. Phys. Chem. B* **2010**, *114*, 7348−7358.
(42) Bai, Y.; Greenfeld, M.; Travers, K. J.; Chu, V. B.; Lipfert, J.; Doniach, S.; Herschlag, D. Quantitative and Comprehensive Decomposition of the Ion Atmosphere around Nucleic Acids. *J. Am. Chem. Soc.* **2007**, *129*, 14981−14988.
(43) Yoo, J.; Aksimentiev, A. Competitive Binding of Cations to Duplex DNA Revealed through Molecular Dynamics Simulations. *J. Phys. Chem. B* **2012**, *116*, 12946−12954.
(44) Cheng, Y.; Korolev, N.; Nordenskiold, L. Similarities and Differences in Interaction of K+ and Na+ with Condensed Ordered DNA. A Molecular Dynamics Computer Simulation Study. *Nucleic Acids Res.* **2006**, *34*, 686−696.
(45) Gurtovenko, A. A.; Vattulainen, I. Effect of Nacl and Kcl on Phosphatidylcholine and Phosphatidylethanolamine Lipid Membranes: Insight from Atomic-Scale Simulations for Understanding Salt-Induced Effects in the Plasma Membrane. *J. Phys. Chem. B* **2008**, *112*, 1953−1962.
(46) Joshi, H.; Maiti, P. K. Structure and Electrical Properties of DNA Nanotubes Embedded in Lipid Bilayer Membranes. *Nucleic Acids Res.* **2018**, *46*, 2234−2242.
(47) Case, D. A. et al. *AMBER 14*, University of California, San Francisco: 2014.
(48) Gopfrich, K.; Li, C. Y.; Ricci, M.; Bhamidimarri, S. P.; Yoo, J.; Gyenes, B.; Ohmann, A.; Winterhalter, M.; Aksimentiev, A.; Keyser, U. F. Large-Conductance Transmembrane Porin Made from DNA Origami. *ACS Nano* **2016**, *10*, 8207−8214.
(49) Jo, S.; Kim, T.; Iyer, V. G.; Im, W. Charmm-Gui: A Web-Based Graphical User Interface for Charmm. *J. Comput. Chem.* **2008**, *29*, 1859−1865.
(50) Jorgensen, W. L.; Chandrasekhar, J.; Madura, J. D.; Impey, R. W.; Klein, M. L. Comparison of Simple Potential Functions for Simulating Liquid Water. *J. Chem. Phys.* **1983**, *79*, 926−935.
(51) Humphrey, W.; Dalke, A.; Schulten, K. Vmd: Visual Molecular Dynamics. *J. Mol. Graphics* **1996**, *14*, 33−38.
(52) Feller, S. E.; Zhang, Y. H.; Pastor, R. W.; Brooks, B. R. Constant-Pressure Molecular-Dynamics Simulation - the Langevin Piston Method. *J. Chem. Phys.* **1995**, *103*, 4613−4621.
(53) Martyna, G. J.; Tobias, D. J.; Klein, M. L. Constant-Pressure Molecular-Dynamics Algorithms. *J. Chem. Phys.* **1994**, *101*, 4177−4189.
(54) Sindhikara, D. J.; Kim, S.; Voter, A. F.; Roitberg, A. E. Bad Seeds Sprout Perilous Dynamics: Stochastic Thermostat Induced Trajectory Synchronization in Biomolecules. *J. Chem. Theory Comput.* **2009**, *5*, 1624−1631.
(55) Hart, K.; Foloppe, N.; Baker, C. M.; Denning, E. J.; Nilsson, L.; MacKerell, A. D. Optimization of the Charmm Additive Force Field for DNA: Improved Treatment of the Bi/Bii Conformational Equilibrium. *J. Chem. Theory Comput.* **2012**, *8*, 348−362.
(56) Yoo, J.; Aksimentiev, A. New Tricks for Old Dogs: Improving the Accuracy of Biomolecular Force Fields by Pair-Specific Corrections to Non-Bonded Interactions. *Phys. Chem. Chem. Phys.* **2018**, *20*, 8432−8449.
(57) Yoo, J.; Aksimentiev, A. Improved Parameterization of Amine-Carboxylate and Amine-Phosphate Interactions for Molecular Dynamics Simulations Using the Charmm and Amber Force Fields. *J. Chem. Theory Comput.* **2016**, *12*, 430−443.
(58) Yoo, J. J.; Aksimentiev, A. Improved Parametrization of Li+, Na+, K+, and Mg2+ Ions for All-Atom Molecular Dynamics Simulations of Nucleic Acid Systems. *J. Phys. Chem. Lett.* **2012**, *3*, 45−50.
(59) Vanommeslaeghe, K.; MacKerell, A. D. Automation of the Charmm General Force Field (Cgenff) I: Bond Perception and Atom Typing. *J. Chem. Inf. Model.* **2012**, *52*, 3144−3154.
(60) Phillips, J. C.; Braun, R.; Wang, W.; Gumbart, J.; Tajkhorshid, E.; Villa, E.; Chipot, C.; Skeel, R. D.; Kale, L.; Schulten, K. Scalable Molecular Dynamics with Namd. *J. Comput. Chem.* **2005**, *26*, 1781−1802.
(61) Miyamoto, S.; Kollman, P. A. Settle - an Analytical Version of the Shake and Rattle Algorithm for Rigid Water Models. *J. Comput. Chem.* **1992**, *13*, 952−962.
(62) Andersen, H. C. Rattle - a Velocity Version of the Shake Algorithm for Molecular-Dynamics Calculations. *J. Comput. Phys.* **1983**, *52*, 24−34.
(63) Roe, D. R.; Cheatham, T. E. Ptraj and Cpptraj: Software for Processing and Analysis of Molecular Dynamics Trajectory Data. *J. Chem. Theory Comput.* **2013**, *9*, 3084−3095.

DOI: 10.1021/acs.langmuir.8b02271
Langmuir 2018, 34, 15084−15092